Ni/Al coprecipitated catalysts modified with magnesium and copper for the catalytic steam reforming of model compounds from biomass pyrolysis liquids

F. Bimbela [a], D. Chen [b], J. Ruiz [a], L. García [a,*], J. Arauzo [a]

[a] *Thermochemical Processes Group (GPT), Aragon Institute of Engineering Research (I3A), Universidad de Zaragoza, Mariano Esquillor S/N, 50018 Zaragoza, Spain*
[b] *Department of Chemical Engineering, Norwegian University of Science and Technology (NTNU), N-7491, Trondheim, Norway*

ABSTRACT

Ni/Al coprecipitated catalysts modified with magnesium and copper have been prepared by a constant pH technique and tested in the catalytic steam reforming of model compounds (acetic acid, acetol and butanol) from biomass pyrolysis liquids at 650 °C and atmospheric pressure. Catalysts with different copper contents, reduced at 650 °C for 1 h, were tested in the steam reforming of acetic acid with a steam/carbon (S/C) molar ratio of 5.6. The best performance and the highest hydrogen yield in these conditions were achieved with the 5% Cu catalyst. This catalyst reduced at 650 °C during 10 h showed a high activity, close to the thermodynamic equilibrium, and a stable performance during 12 h in the steam reforming of acetic acid with a S/C = 5.6, using a short space time of 1.00 g catalyst min/g acetic acid. Copper as a promoter produces counterbalanced effects: a decrease in the initial reforming activity and an enhancement of the catalyst stability. The initial steam reforming activity decreased and the CH_4 yield increased concurrently with increasing the copper content, because of the Ni dilution effect. Copper has a positive effect inhibiting the formation of encapsulating coke, identified as the cause for deactivation in acetic acid steam reforming with a steam-to-carbon molar ratio (S/C) of 5.6. However, such a positive effect of copper has not been observed in acetic acid steam reforming with S/C = 14.7 or in the steam reforming of acetol and butanol.

© 2012 Elsevier B.V. All rights reserved.

1. Introduction

Biomass pyrolysis liquids, also named bio-oil, constitute a valuable product offering numerous possibilities for the production of a variety of chemicals and as a fuel [1–4]. This bio-oil or its fractions can also be upgraded to different chemicals, to a syngas and/or to energy [4–6]. In this context, catalytic steam reforming constitutes an alternative for hydrogen and syngas production [7].

Given the complex composition of bio-oil [8,9], model compounds have usually been selected to gain insight into the catalytic steam reforming of bio-oil oxygenates. Acetic acid [7,10–31], acetone [13,21,32,33], acetol [28,34,35], methanol [7], ethanol [13], ethylene glycol [32] and 1-butanol [35] have been selected as representative of the oxygenates in the aqueous fraction of bio-oil.

The catalysts used in the steam reforming process are usually nickel based, either commercial [7,11,19,36–41] or synthesized in different laboratories [12,16,20,22,23,25,26,28,29,33,34,39–42]. Nevertheless, some authors have also investigated noble metal based catalysts [13,17,18,23–25,30,33,43]. The main advantages of Ni catalysts are their high activity and selectivity to hydrogen,

as well as their relatively low cost compared to other catalysts based on noble metals. However, there still remains the challenge of developing nickel based catalysts with sufficient resistance to deactivation by coke deposition.

In our previous works [20,35], the catalytic steam reforming of model compounds from the aqueous fraction of bio-oil, acetic acid [20], acetol and 1-butanol [35], was studied using Ni/Al coprecipitated catalysts. The results led to the selection of the most appropriate Ni load (28%) for further catalyst preparations.

In the present work, Ni/Al coprecipitated catalysts with a different preparation technique are evaluated, incorporating promoters which might mitigate the deactivation caused by coke deposition. Magnesium and copper have been selected as promoters.

Mg has been studied as a promoter of Ni-Al catalysts in processes such as dry reforming of methane [44], catalytic decomposition of methane [45] or steam reforming of natural gas [46] and methane [47]. Mg as a promoter of Ni-Al catalysts has also been investigated in the catalytic gasification of biomass [48], catalytic steam reforming of model compounds of bio-oil [28], and catalytic steam reforming of bio-oil [23,40].

Mg was chosen as a textural promoter due to the basicity of MgO, which hinders carbon deposition through gasification of the deposits, thus increasing the catalyst stability. Mg enhances steam adsorption capability and solid solutions of NiO/MgO stabilize

nickel and prevent catalyst sintering [40]. Although magnesium favors coke removal by gasification [23,47], some authors have reported deactivation by coke [45]. Other authors indicated that the addition of magnesium caused the formation of more easily oxidized coke and with higher hydrogen content [46]. The addition of this promoter results in the neutralization of the acidity of the support, restraining polymerization reactions [49].

Cu as a promoter in Ni-Al catalysts has been employed in the thermal decomposition of methane for the production of both hydrogen and carbon nanofibers or carbon nanotubes [45,50–61]. Mariño et al. [62–65] used Cu impregnated catalysts on γ-Al$_2$O$_3$ modified with Ni and K in the steam reforming of ethanol at low temperatures (around 300 °C).

Copper was chosen as a promoter because it is an active metal with a carbon–metal bonding energy lower than that of nickel. This allows a less strong adsorption of reactant molecules, and therefore the destabilizing of the precursors for coke formation over the metal active sites. Copper has been shown to promote activity in the thermal decomposition of methane [53], and the presence of copper is favorable to the gasification of the carbon formed in methane decomposition [55]. Other authors have concluded that Cu inhibited the formation of encapsulation coke [58] and also the formation of graphite layers [50].

Magnesium has been proved to have a positive effect on the catalytic steam reforming of model compounds of bio-oil, but there are few studies using copper in this context [66]. The presence of these two promoters in the catalyst could have some synergic effects resulting in a stable catalyst resistant to coke deactivation.

The present work deals with the effects of the presence of Cu in Ni-Cu-Mg-Al catalysts on their activity, selectivity and stability during the steam reforming of the model molecules from the aqueous fraction of bio-oil, such as acetic acid, acetol and butanol, at 650 °C.

2. Experimental

2.1. Experimental system

The experimental system is a micro-reactor test facility developed and manufactured by PID Eng&Tech. It consists of a fixed bed placed inside a tubular quartz reactor of 9 mm (i.d.). The height of the bed is about 25 mm. The bed is a mixture of sand, used as inert filler, and a Ni coprecipitated catalyst, with a total bed weight of around 1.8 g. The catalyst/sand weight ratio ranged from 0.01 to 0.03 in the different runs. The particle sizes of both catalyst and sand are between 106 and 250 μm. A more detailed description of the setup can be found elsewhere [20].

The experimental system was operated at atmospheric pressure and the organics tested were fed as aqueous solutions. The nitrogen flow rate was fixed at 40 cm^3 (STP)/min.

2.2. Chemicals

Acetic acid was supplied by PANREAC (99.5% purity), acetol (hydroxyacetone), tech. (97.5%) by Sigma-Aldrich and 1-butanol, reagent grade (99.5%), was provided by Scharlau. Other chemicals used included commercial gases at purity >99.999%: hydrogen, nitrogen, air, helium and argon, as well as a standard gas mixture (N$_2$, H$_2$, CO$_2$, CO, CH$_4$ and C$_2$s) for the calibration of the gas chromatograph.

2.3. Catalyst preparation

Five different Ni-Al-Mg catalysts were prepared with different copper percentages in the formulation (0, 1, 3, 5 and 10% by

weight). The preparation method was adapted from patents by Bhattacharyya et al. [67] and has been successfully employed in the preparation of Ni coprecipitated catalysts with pure hydrotalcite-like structures and promoters such as Fe [68] or Co [49]. The Ni/(Ni + Al + Mg + Cu) was set at 28% by weight value, in order to establish the active metal loading in all the preparations. This nickel content was selected from previous works [20,35]. A x = Al/(Ni + Al + Mg + Cu) molar ratio of 0.25 was also fixed, since it has been reported in the literature that values for this ratio ranging between 0.20 and 0.33 enable the formation of pure hydrotalcite structures [49,68].

The preparation method consists of the coprecipitation by dropwise addition of the solution containing the metallic nitrates (Ni(NO$_3$)$_2$·6H$_2$O, Mg(NO$_3$)$_2$·6H$_2$O, Cu(NO$_3$)$_2$·3H$_2$O and Al(NO$_3$)$_3$·9H$_2$O) on a basic solution of sodium carbonate (Na$_2$CO$_3$) and sodium hydroxide (NaOH). The amounts of these two chemicals have been calculated to yield stoichiometric excess of hydroxides and carbonates of 0 and 50% respectively. The preparation is performed in N$_2$ inert atmosphere with continuous stirring. After the addition of the metallic salts the pH of the solution is adjusted with acid to a value of 8.5 and aged for 15 h at 80 °C. After filtering and washing to eliminate the Na cations, the precursor is dried overnight at 105 °C. Finally, the hydrated precursor is milled and sieved (particle size ranging from 106 to 250 μm) previous to calcination in air flow, following a heating rate of 5 °C/min up to 600 °C. The calcination temperature is held at 600 °C for 6 h.

2.4. Catalyst characterization

The elemental analysis of the catalysts was done by means of optical emission spectrometry with inductively coupled plasma (ICP-OES, Thermo Elemental IRIS INTREPID RADIAL, equipped with a Timberline IIS automatic). The calcined precursors were dissolved in nitric acid diluted with deionized water.

The XRD analyses were done with a Rigaku D/Max-B System diffractometer. A copper anode was employed, choosing the wavelength corresponding to copper (λ = 1.5418 Å) by means of a graphite monochromator. The measurements were completed in the 2θ range from 5° to 90° with a scanning rate of 0.030°/s.

The temperature-programmed reduction (TPR) analyses were done with a setup consisting of a quartz reactor heated by an electrical furnace at a heating rate of 10 °C/min in a mixture containing 7 mol% H$_2$ in Ar, from room temperature up to a final temperature of 900 °C. Hydrogen consumption was measured by analyzing the effluent by means of a thermal conductivity detector. The steam formed during the reduction was removed by a cooling trap. The sample weight was 300 mg approx.

The nitrogen adsorption measurements were done in a TRISTAR II 3000 V6.08A analyzer from MICROMERITICS.

The X-ray photoelectron spectroscopy (XPS) analyses were obtained by means of a KRATOS AXIS ULTRA DLD spectrometer, with monochromatic Al Kα ($h\upsilon$ = 1486.71 eV) as the X-ray source. A kinetic energy of 20 eV was used to collect core-level spectra. The charge effects have been corrected by using the C 1s peak at 284.9 eV. The relative atomic concentrations obtained with the software have been calculated by means of the atomic sensitivity factors technique.

Hydrogen chemisorption measurements were performed with a MICROMERITICS ASAP 2010C. 200 mg of the calcined precursor were introduced into a U-shaped quartz reactor, confined between two quartz wool plugs to prevent the samples from being swept away. The hydrogen chemisorption was studied at 35 °C, after preliminary reduction of the calcined precursors at 650 °C with H$_2$ diluted in Ar (7 vol.%). Three reduction times, 1, 8 and 10 h, were taken into consideration for the majority of the catalysts, and some catalysts were also tested for 12 h. A spherical model for the metallic

Table 1
Results of the elemental analyses of the different catalysts (metal contents are expressed as wt.%).

Sample	%Ni		%Cu		%Al		%Mg	
	Nominal	Analytical	Nominal	Analytical	Nominal	Analytical	Nominal	Analytical
0% Cu	28	30.1	0	0.1	14.3	18.1	27.1	21.5
1% Cu	28	29.6	1	1.2	14.3	17.3	26.6	22.1
3% Cu	28	28.4	3	3.3	14.2	16.8	25.5	22.1
5% Cu	28	28.8	5	5.5	14.0	16.7	24.4	20.6
10% Cu	28	26.6	10	11.5	13.8	14.8	21.7	20.5

particles and a H/Ni adsorption stoichiometry of 1 were assumed in calculating the Ni surface area.

Temperature programmed oxidation analyses of some used samples were conducted from room temperature through 900 °C to characterize the carbon deposited on the catalyst surface. The sample was heated at a rate of 10 °C/min using oxygen:argon (30:70) with an argon flow of 30 STP cm^3/min. The amount of CO_2 released was measured by mass spectrometry.

Scanning electron microscopy (SEM) images from some of the used samples were taken with a JEOL-JSM 6400 scanning electron microscope using an augmentation of 10,000 times.

2.5. Catalytic tests

Experiments were carried out at 650 °C. The majority of them had a time-on-stream of 2 h, except one with 12 h. The model compounds of biomass pyrolysis liquids were acetic acid, acetol and butanol. The S/C molar ratio of the aqueous solutions corresponding to acetic acid and acetol was set at 5.6 because this value is within the range of typical values found for the aqueous fraction of bio-oil in the literature [24,27,36,40]. In the case of 1-butanol, an aqueous solution was prepared with a S/C ratio of 14.7, a value which is close to the maximum solubility of 1-butanol in water at room temperature [69].

Some experiments were also performed with an aqueous solution of acetic acid having a S/C ratio equal to 14.7. In the literature the effect of the S/C ratio in the catalytic steam reforming of acetic acid [7,11,15,16,19,22] has normally been studied for values of between 2 and 7.5, except for Basagiannis and Verykios [16] who studied two lower S/C values (0.75 and 1.5). It was considered of interest to study greater values of the S/C ratio to determine its effect on catalyst deactivation.

Acetic acid experiments using a S/C ratio equal to 5.6 were carried out using a liquid feeding rate of 0.228 mL/min and a catalyst weight of 53.9 mg. In the runs with a S/C ratio of 14.7, the catalyst weight was fixed at 22.7 mg and the liquid feeding rate at 0.218 mL/min.

Thus, the catalyst weight/acetic flow rate ratio (W/m_{HAc}) was around 1.00 g catalyst min/g acetic acid in all the runs, and the $G_{C1}HSV$ was around 42,000 h^{-1}. The $G_{C1}HSV$ is defined as the volume of C_1-equivalent species in the feed at standard temperature and pressure per unit volume of catalyst (including the void fraction) per hour [11]. Such a definition permits a comparison of the activity of the catalysts when using feedstocks with a varying number of carbon atoms, being especially useful in the case of complex feedstocks such as bio-oil.

The effect of the copper content was investigated in the catalytic steam reforming of acetic acid using 0, 1, 3, 5 and 10% Cu catalysts.

In the case of acetol and butanol as model compounds, 0% and 5% Cu catalysts were used. The catalytic steam reforming of acetol was studied employing a W/m_{Ac} of 0.53 g catalyst min/g acetol, which corresponds to a $G_{C1}HSV = 95,000$ h^{-1}, using 18.1 mg of catalyst and a liquid feeding rate of 0.17 mL/min. The catalytic steam reforming of butanol was carried out with a W/m_{But} equal to 1.00 g

catalyst min/g butanol ($G_{C1}HSV = 67,000$ h^{-1}, 14.6 mg of catalyst and 0.23 mL/min of liquid feeding rate).

The experimental conditions employed, especially the $G_{C1}HSV$ values, were selected for the purpose of catalyst comparison.

The experimental procedure involved previous in situ reduction of the catalyst, with hydrogen diluted in nitrogen (10%, v/v) at a fixed temperature of 650 °C. These reduction conditions were taken from a previous work [20]. The reduction time was 1 h in the study of the effect of the Cu content and 10 h in the rest of the runs.

The overall results corresponding to the different catalytic steam runs conducted are presented in the tables. These overall results have been calculated during the time-on-stream of the experiments, 2 h of reaction (except for the 12 h TOS run).

Gas and liquid yields are expressed as g of product divided by the feed (aqueous solution of the organic compound) and indicate the overall yields obtained. The sum of gas and liquid yields is called recovery and provides information about mass balance closure. The liquid products from the reaction were weighed but no chemical analysis of those liquids was carried out. The gas products were analyzed by gas chromatography. Carbon conversion corresponds to the carbon in the feed that is converted into gases. Overall yields to different gases are expressed as g of gas divided by g of organic fed. Overall gas composition is expressed on a N_2 water free basis. The evolution of yields to different gases (H_2, CO and CH_4) versus time is shown in the figures.

The corresponding equilibrium values have been calculated with Aspentech HYSYS 3.2 simulation software. A Gibbs reactor module with a PRSV thermodynamic package and the expected compounds (H_2, CO, CO_2, CH_4, C_2, C_3, acetone, ketene, etc.) together with the model compounds (acetic acid, acetol and butanol) have been input. The Gibbs reactor module computes the outlet stream composition using the condition that the Gibbs free energy of the reaction system is at a minimum at equilibrium. No reaction stoichiometry is required.

3. Results and discussion

3.1. Catalyst characterization

3.1.1. Elemental analysis by ICP-OES

Table 1 shows a comparison of the nominal and analytical values determined with the elemental analyses. The Ni and Cu contents have a good concordance between the nominal and the analytical values, except the Ni content in the 0 and 1% Cu samples. The Al content exceeds the nominal values in all cases, unlike the Mg content which is below the nominal, indicating that Mg was not completely incorporated into the hydrated precursors. This might be a result of a localized re-dissolving phenomenon of $Mg(OH)_2$ during the adjustment of the pH with acid during the preparation. The values for the $x = Al/(Ni + Al + Mg + Cu)$ molar ratio have also been calculated from these results. All the x values obtained are within the range necessary to obtain pure hydrotalcite structures (0.2–0.33) [68], though the analytical values calculated were a little higher than the nominal x value of 0.25.
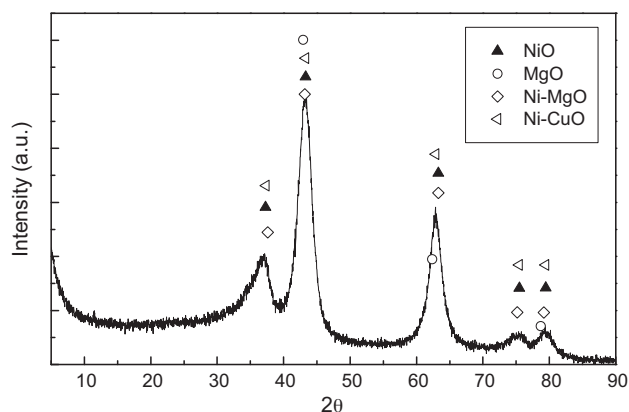
Fig. 1. XRD pattern of the precursor for the 5 wt.% Cu catalyst calcined at 600 °C.

Fig. 2. TPR profiles of the catalysts. TPR conditions: 300 mg sample weight, 7 mol% H_2/Ar, heating rate of 10 °C/min, 900 °C final temperature.

3.1.2. XRD analysis

All the patterns corresponding to the calcined precursors are very similar. Thus, as an example, only the pattern corresponding to the 5% Cu calcined precursor is depicted in Fig. 1. All the XRD patterns of the catalysts prepared show broad and asymmetric peaks. A comparison of the different sample patterns with those of standard patterns corresponding to inverse spinel $NiAl_2O_4$, $MgAl_2O_4$, α-Al_2O_3, γ-Al_2O_3, NiO, CuO, MgO, Ni-Mg-O and Ni-Cu-O solid solutions shows that all the calcined samples contain the possible Ni and Mg oxides and/or Ni-Mg and Ni-Cu mixed oxides. The overlapping of the peaks of these possible oxides or mixed oxides and the wide diffraction peaks of the samples hinders a clear identification of the actual crystalline phases in the calcined samples. The crystalline phases corresponding to CuO, $MgAl_2O_4$, $NiAl_2O_4$, α-Al_2O_3 and γ-Al_2O_3 were not detected. It is also noticeable that no significant differences are found in terms of phases detected or in the crystallinity of the catalysts with increasing Cu contents.

It has not been possible to elucidate whether the absence of CuO crystalline phases in the XRD patterns is a result of the formation of Ni-Cu mixed oxides or due to the presence of CuO as an amorphous phase.

The reported phases of the Cu promoted Ni-Al catalysts in the literature are controversial [45,53,60]. The absence of visible peaks corresponding to CuO and $NiAl_2O_4$ has also been reported by Li et al. [53]. The well-crystallized precipitated precursor with a Feitknecht compound structure produced a strong interaction between the composing oxides after calcinations carried out at 450 °C. Ashok et al. [60] could only detect crystalline CuO at high Cu contents (32 wt.%). Spinel-like structures of $NiAl_2O_4$ and $MgAl_2O_4$ as well as crystalline CuO were detected in the work of Monzón et al. [45] for NiCuMgAl catalysts prepared by coprecipitation at constant pH. In that work, catalysts with 14 wt.% Ni and 14 wt.% Cu were prepared and the calcination conditions were 800 °C for 11 h in N_2 atmosphere.

The discrepancy can be explained by the effect of the calcination temperature and time on the phase composition. Thus, an increase in the calcination temperature implies a greater tendency towards the formation of the spinel phase and a significant diminution of the NiO phase [48,70–72]. The increase in the calcination time can also contribute in the same way [70].

3.1.3. Temperature-programmed reduction (TPR)

Fig. 2 shows the TPR profiles of the 0, 1, 3, 5 and 10% Cu calcined precursors. The 0% Cu sample had a single peak with a maximum at 850 °C, which is higher than that corresponding to a homologous catalyst prepared by coprecipitation at increasing pH, 28% relative at.% of nickel without magnesium [20]. This might be ascribed to the presence of MgO in the catalysts. The calcined precursor would
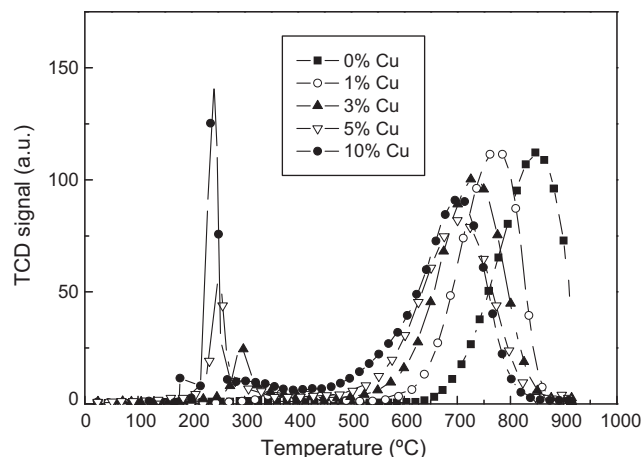
be constituted by a solid solution of mixed oxides of the different metals, particularly NiO·MgO, which is more difficult to reduce.

In the catalysts containing copper, two peaks can be observed: one at low temperatures, around 250–300 °C, ascribed to the reduction of Cu species, and the other at higher temperatures, between 650 and 750 °C, corresponding to the reduction of Ni containing species present in the different catalysts prepared. When the copper content increases, the low temperature peaks are enlarged and the high temperature peaks become smaller. The maximum of both low and high temperature peaks are shifted to lower temperatures.

The Ni catalyst without copper has a very high maximum reduction temperature (850 °C). The possible existence of a solid solution of mixed oxides is consistent with the observations of Moliner et al. [59]. This is also in agreement with Monzón et al. [45], who state that Mg and Al oxides do not reduce below 900 °C and remark on the strong interaction of the nickel with the neighboring metals to explain the higher temperature of the reduction peak when compared to pure black NiO.

In the TPR analyses reported in the literature for Ni-Cu-Al catalysts [45,53,57,58,60], the low temperature peak is associated to the reduction of Cu species, ($Cu^{II} \rightarrow Cu^0$) whereas the high temperature reduction region is attributed to the reduction of Ni ($Ni^{II} \rightarrow Ni^0$). From Fig. 2 it can be concluded that adding 1 wt.% of Cu significantly changed the catalyst reduction, where the maximum temperature of the main reduction peak was reduced from 850 °C to 773 °C. There is only one reduction peak and no obvious CuO reduction peak was observed. This could suggest a Ni–Cu alloy formation. When CuO increased to 3 wt.%, the main reduction peak further shifted to a lower temperature (727 °C), but a small peak appeared at low temperatures, around 300 °C. Upon a further increase in the amount of Cu, the low temperature reduction peak increased, and the peak also shifted to a lower temperature. This fact suggests that there is a Cu rich phase existing at the highest Cu contents. The possible Ni atoms coordinated with Cu atoms in the Cu rich phase could decrease the reduction temperature. The maximum reduction temperature of the Ni-rich phase is almost identical for 5 and 10% Cu catalysts (ca. 705 °C). Because the area corresponding to the Ni-rich phase is similar for these catalysts, it indicates that the amount of Ni-rich phase did not increase. For the 10% Cu catalyst (Fig. 2), the increase in the Cu amount with respect to that of the 5% Cu catalyst increased only the amount of the Cu-rich phase.

Li et al. [53] indicate that it is not reasonable to say that the two metals, Ni and Cu, form an alloy although significant changes are observed in the reduction performance. Because we have not

Table 2
Results of the N_2 adsorption measurements for the calcined precursors.

Catalyst	BET surface area (m^2/g)	Average pore diameter (nm)	Specific pore volume (cm^3/g)
0% Cu	146	8.5	0.34
1% Cu	178	9.9	0.52
3% Cu	171	11.1	0.55
5% Cu	186	9.8	0.53
10% Cu	169	7.5	0.38

Table 3
Comparison of the Cu/Ni atomic ratio and the Mg/Ni atomic ratio from the results of the XPS and ICP-OES analyses with the nominal values for the calcined precursors.

Catalyst	Cu/Ni atomic ratio			Mg/Ni atomic ratio		
	XPS	ICP-OES	Nominal	XPS	ICP-OES	Nominal
0% Cu	0	0.00	0	1.73	1.73	2.34
1% Cu	0.04	0.04	0.03	1.90	1.80	2.29
3% Cu	0.08	0.11	0.10	1.62	1.88	2.20
5% Cu	0.16	0.18	0.17	1.65	1.73	2.11
10% Cu	0.35	0.40	0.33	1.59	1.86	1.87

demonstrated the existence of Ni–Cu alloys in our catalysts, we prefer to use the terms Cu-rich and Ni-rich phases.

3.1.4. Nitrogen adsorption

The results of the surface area calculations by the BET equation, the average pore diameter and the specific pore volume for these are presented in Table 2.

The BET surface area of the catalysts modified with copper is higher than that of the 0% Cu catalyst. No clear tendency is observed when the copper content increases. The surface areas are consistent with results reported in the literature for Ni-Cu-Al catalysts prepared by coprecipitation [52,60]. Ashok et al. [60] found a decline in surface area with increasing Cu content, but they attributed this fact to the decrease in the aluminum content. In the present case, the variation of the aluminum content is very small.

3.1.5. X-ray photoelectron spectroscopy (XPS)

Table 3 shows the theoretical Cu/Ni and Mg/Ni atomic ratios and the empirical values calculated both from the results of the ICP-OES and XPS analyses.

The empirical Cu/Ni atomic ratio on the surface, determined from the XPS data, generally has a good concordance with the nominal values. Regarding Mg, all the catalysts are far below the nominal Mg/Ni ratio, probably indicating that Mg is not adequately incorporated into the catalyst, as confirmed by the ICP-OES analyses (Table 1). The empirical Mg/Ni atomic ratios calculated both from the ICP-OES and the XPS data are quite similar, the lowest being those determined by XPS for copper contents higher than 1 wt.%. This could indicate that Mg is mainly located in the bulk of the catalyst particles and not on the surface.

The binding energies (B.E.) corresponding to Ni 2p$^{3/2}$ and Cu 2p$^{3/2}$ have been analyzed. The presence of NiO is confirmed by a primary peak at 855 eV along with a secondary peak at 862.2 eV, in accordance with the literature [73]. In the case of 1 and 3% Cu catalysts, the B.E. of the primary peak of Cu is found at 933.2 eV, whereas

for 5 and 10% Cu the B.E. are 933.8 and 933.5 eV, respectively. Thus, this increase in the binding energies helps demonstrate the presence of a Cu-rich phase on the catalyst surface, in agreement with the TPR results.

3.1.6. Hydrogen chemisorption

Table 4 lists the results obtained in the H_2-chemisortion study, carried out with different reduction times. The experimental error ($\pm 2\sigma$) of the Ni surface area is ± 0.5 m^2/g. The Ni surface area significantly increases for the 0% Cu sample when the reduction time increased from 1 to 12 h, an indication that the Ni species present in the catalyst do not become massively reduced with 1 h of reduction. For 1% Cu and 3% Cu samples the Ni surface area increases when the reduction time increases from 1 to 10 h. For the 5% Cu sample the Ni surface area increases from 1 to 8 h, but decreases from 8 to 10 h of reduction time. A decrease of Ni surface area is observed when the reduction time increases from 1 h for the 10% Cu sample.

The performance of the 0% Cu sample can be explained considering the TPR characterization results. The reduction peak at 850 °C could indicate the formation of a NiO·MgO solid solution. The increase in the Ni surface area when the reduction time increases could be due to the reduction of this NiO·MgO solid solution, which would generate stable Ni crystallites. The TPR results for the 5% Cu and 10% Cu samples suggest a Ni-rich phase that is easily reduced. When the reduction time increases, more Ni is reduced but the Ni surface area decreases. This could be due to the increase in the Ni crystallite size, indicating that no stable crystallites are generated in this case. For the 1% Cu and 3% Cu samples an intermediate performance is observed. The presence of Cu achieves a more easily reduced phase than that found in the 0% Cu sample, but generates stable Ni crystallites.

The Ni surface area linearly decreases with increasing Cu contents. For 1, 8 and 10 h of reduction time the sample with the greatest Ni surface area is 0% Cu. The catalyst with 10% Cu shows the smallest Ni surface area.

According to the XPS analyses, a significant increase in the Cu/Ni atomic ratio occurs as the Cu content increases, which indicates a higher surface Cu amount. Because Cu does not chemisorb hydrogen due to its weak adsorption and the ready desorption at 25 °C [74], the Ni surface area decreases. As can be observed from the ICP-OES results in Table 1, the Ni content in the samples slightly decreases as the Cu content increases. This also influences the Ni surface area, although probably the higher content of Cu on the surface could have a greater effect.

3.2. Catalytic steam reforming of acetic acid

3.2.1. Effect of the Cu content

Table 5 gives the overall results obtained with Ni based catalysts with different Cu contents, which were reduced at 650 °C for 1 h. The results from the different runs presented in the tables must be analyzed with caution since the data are affected by the deactivation which could lead to erroneous interpretations. In order to overcome this difficulty, the evolution with time of the relevant yields to individual gases is presented in the figures. The greatest carbon conversion to gas was obtained with the 5% Cu catalyst,

Table 4
Results of the hydrogen chemisorption measurements.

Reduction time (h)	0% Cu Ni surface area (m^2/g sample)	1% Cu Ni surface area (m^2/g sample)	3% Cu Ni surface area (m^2/g sample)	5% Cu Ni surface area (m^2/g sample)	10% Cu Ni surface area (m^2/g sample)
1	14.4	13.3	13.5	11.3	8.4
8	19.0	16.3	15.4	14.8	7.9
10	19.4	17.6	16.7	13.6	n/a
12	20.0	n/a	n/a	n/a	7.6

Table 5
Overall results during 2 h of catalytic steam reforming of acetic acid with catalysts reduced during 1 h at 650 °C. Effect of the Cu content. W/m_{HAc} = 1.00 g catalyst min/g acetic acid (G_{C_1}HSV = 41,660 h^{-1}). Catalyst weight: 53.9 mg, liquid feeding rate = 0.22 mL/min, S/C = 5.6.

	Run				
	1	2	3	4	5
Copper content (wt.%)	0	1	3	5	10
Yields (g/g liquid fed)					
Gas	0.150	0.132	0.106	0.278	0.224
Liquid	0.776	0.807	0.842	0.647	0.712
Recovery (gas + liquid)	0.926	0.939	0.948	0.925	0.936
Carbon conversion (%)	43.12	38.37	31.66	81.58	69.42
Gas yields (g/g acetic acid)					
H_2	0.056	0.047	0.037	0.100	0.069
CO	0.058	0.051	0.052	0.136	0.155
CO_2	0.536	0.474	0.367	0.968	0.735
CH_4	0.002	0.003	0.005	0.005	0.014
C_2	0.000	0.000	0.001	0.000	0.001
Gas composition (% mol, N_2 and H_2O free)					
H_2	66.13	65.17	63.89	64.88	60.12
CO	4.94	5.01	6.37	6.29	9.58
CO_2	28.64	29.31	28.61	28.40	28.79
CH_4	0.29	0.51	1.00	0.43	1.48
C_2	0.00	0.00	0.13	0.00	0.03

which also yielded the greatest H_2 and CO_2 yields. The average gas composition is around 65% H_2, 5% CO and 28% CO_2 except for 10% Cu, which has lower H_2 and higher CO contents.

The evolution of H_2 and CO (Fig. 3) and CH_4 (Fig. 4) yields with time can be subjected to analysis. The thermodynamic equilibrium has also been included and appears as horizontal lines. The evolution of the CO_2 yield with time follows the same tendencies as H_2, and thus has not been included.

The general tendency shows that the initial yields of H_2 decrease when the copper content increases, which correlates quite well with the nickel surface area. The analysis of the evolution of yields with time reveals different performances. The 0%, 1% and 3% Cu catalysts show similar decays with time while the 5% and 10% Cu
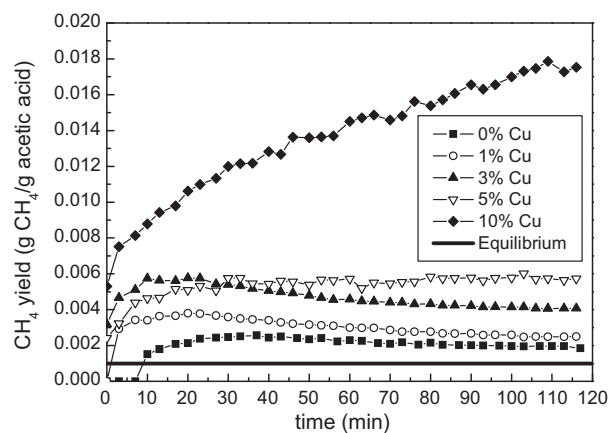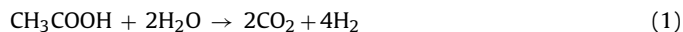
Fig. 3. H_2 and CO yield evolution with time. Catalysts reduced for 1 h. Effect of the Cu content (lines between dots only represent visual aids). T = 650 °C, W/m_{HAc} = 1.00 g catalyst min/g acetic acid, S/C = 5.6.

Fig. 4. CH_4 yield evolution with time. Catalysts reduced for 1 h. Effect of the Cu content (lines between dots only represent visual aids). T = 650 °C, W/m_{HAc} = 1.00 g catalyst min/g acetic acid, S/C = 5.6.

samples depict a very stable performance in H_2 and CO_2 yields throughout, slightly increasing with the reaction time. CO yields decrease for 0%, 1% and 3% Cu catalysts whereas a slight increase can be observed in the 5% and 10% Cu catalysts.

The general tendency shows that at the beginning of the experiments and after 2 h of reaction, the increase in copper content increases methane production. For the 10% Cu catalyst a continuous increase in the CH_4 yield is observed over time.

The reactions taking place in the catalytic steam reforming of oxygenates from the aqueous fraction of bio-oil, which were first detailed in Wang et al. [11], can explain these results. Also, Basagiannis and Verykios [16] presented the overall reaction system that may take place in the steam reforming of acetic acid over a wide temperature range. The reactions that may take place are:
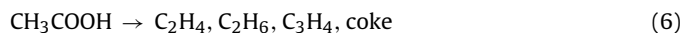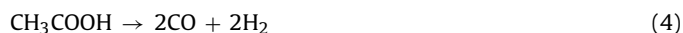
Acetic acid steam reforming:

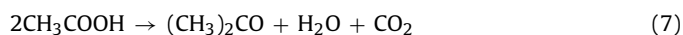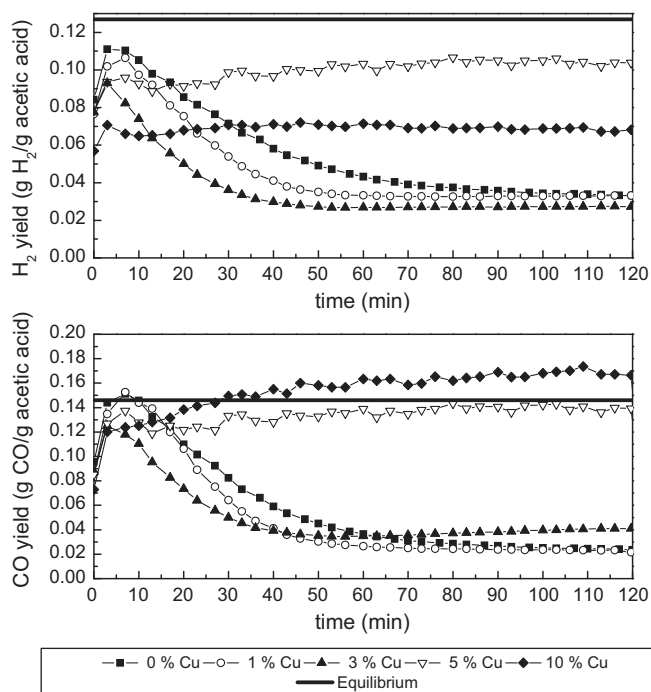$$CH_3COOH + 2H_2O \rightarrow 2CO_2 + 4H_2 \tag{1}$$

Methane steam reforming:

$$CH_4 + H_2O \Leftrightarrow CO + 3H_2 \tag{2}$$

Water gas shift (WGS) reaction:

$$CO + H_2O \Leftrightarrow CO_2 + H_2 \tag{3}$$

Thermal decomposition:

$$CH_3COOH \rightarrow 2CO + 2H_2 \tag{4}$$

$$CH_3COOH \rightarrow CH_4 + CO_2 \tag{5}$$

$$CH_3COOH \rightarrow C_2H_4, C_2H_6, C_3H_4, coke \tag{6}$$

Ketonization:

$$2CH_3COOH \rightarrow (CH_3)_2CO + H_2O + CO_2 \tag{7}$$

Dehydration:

$$CH_3COOH \rightarrow CH_2CO + H_2O \tag{8}$$

Methanation:

$$CO + 3H_2 \Leftrightarrow CH_4 + H_2O \tag{9}$$

$$CO_2 + 4H_2 \Leftrightarrow CH_4 + 2H_2O \tag{10}$$

Boudouard reaction:

$$2CO \Leftrightarrow C + CO_2 \tag{11}$$

Steam gasification of carbon deposits [16]:

$$C + H_2O \rightarrow CO + H_2 \tag{12}$$

At a reaction temperature of 650 °C with catalyst the predominating reactions are (1), (2) and (3). Methane may be generated from the thermal decomposition of the oxygenate (reaction (5)) and also from reactions (9) and (10). The generation of methane has been indicated as being a sign of catalyst deactivation [75], which would suggest that methane is probably generated from the thermal decomposition (5) on the deactivated catalyst surface and not via methanation.

In order to elucidate this, the results were compared to those of non-catalytic experiments from a previous work [20]. In the non-catalytic experiments at 650 °C, the runs were carried out at similar operating conditions, but the reaction bed was only constituted by sand particles. The overall carbon conversion to gas during 2 h was low, only up to 3%, but the methane content in the gas composition was noticeable, and also that of C_2 (mainly C_2H_4 and C_2H_6). The overall gas composition (mol%, N_2 and H_2O free) during 2 h in the non-catalytic experiment at 650 °C was: 37.3% H_2, 17.3% CO, 26.7% CO_2, 16.8% CH_4 and 1.9% C_2. These results could corroborate the suggestion that $CH9_4$ is produced from the thermal decomposition of acetic acid (5) rather than from the methanation reactions ((9) and (10)). Thus, the presence of the catalyst would favor the steam reforming of methane but, as the deactivation of the catalyst proceeds, the yield to methane would increase with reaction time.

The CH_4 yield increases when the copper content increases in the catalysts. It is possible that the Cu-rich phase that increases with the Cu content hinders the CH_4 steam reforming reaction (2).

Therefore, the evolution of H_2, CO, CO_2 and CH_4 yields with time for 0% Cu, 1% Cu and 3% Cu indicates the loss of catalyst activity in reactions (1)–(3). TPR analyses showed that increasing copper contents significantly enhanced the reduction of the Ni species, lowering the temperature at which the catalysts become quantitatively reduced. Thus, 5% and 10% Cu would be easier to reduce and become activated under the reforming conditions. However, 0% Cu, 1% Cu and 3% Cu catalysts are more difficult to reduce and do not maintain their activity in the steam reforming of acetic acid. This fact could be the cause of the decrease in H_2, CO and CO_2 yields with time for these catalysts.

If it is assumed that Ni is the sole active metal for the C—C bond cleavage in Ni-Cu-Al catalysts, as proposed in the literature [65], an increase in copper content would imply a decrease in the catalyst reforming activity. On the other hand, 5% and 10% Cu catalysts would be more activated as a result of the enhancement with increasing Cu contents of the reduction of Ni species, an active metal for C—C bond rupture [64], thus yielding greater reforming activity. The stable performance throughout in this case could be explained by the role of Cu in inhibiting the deactivation by deposition of encapsulating coke on the surface. This results in greater conversion and H_2 and CO_2 yields for 5% Cu as a result of a lower Cu content which is inactive for steam reforming, in agreement with the observations of Monzón et al. [45].

The superior activity of the 5% Cu catalysts compared to the 10% Cu could be explained as a consequence of the Ni dilution effect caused by the higher Cu load in the 10% Cu. In the TPR results, it was observed that an increase in the Cu content from 5% to 10% resulted in an increase in the Cu-rich phase, having little effect on the Ni-rich phase. In addition, the XPS and H_2 chemisorption analyses reveal a higher surface Cu/Ni ratio and lower Ni surface area in the 10% Cu, which could be responsible for the inferior performance of 10% Cu. The Cu would not catalyze the acetic acid steam reforming reaction (1) which involves C—C bond ruptures. The initial yield to H_2 expressed per g of catalyst was calculated from the data presented in Fig. 3. This yield diminished with increasing Cu contents (0.055 mol H_2/(min g_{cat}) for 0% Cu through 0.035 mol H_2/(min g_{cat}) for 10% Cu). Nevertheless, if the initial yield to H_2 is expressed per m^2 of Ni, based on the Ni surface area data from chemisorption after 1 h of reduction (Table 4), the values obtained are very similar

Table 6
Overall results during 2 h of catalytic steam reforming of acetic acid using 0% and 5% Cu catalysts. Reduction 10 h at 650 °C.

| | Run | | | | |
	6	7	8	9	10
Copper content (%)	0	5	5	0	5
S/C	5.6	5.6	5.6	14.7	14.7
Reaction time (h)	2	2	12.25	2	2
Yields (g/g liquid fed)					
Gas	0.234	0.343	0.334	0.139	0.115
Liquid	0.695	0.623	0.604	0.804	0.838
Recovery (gas + liquid)	0.929	0.967	0.938	0.943	0.953
Carbon conversion (%)	67.25	100.13	97.6	87.31	73.13
Gas yields (g/g acetic acid)					
H_2	0.087	0.127	0.122	0.133	0.102
CO	0.101	0.161	0.156	0.074	0.076
CO_2	0.828	1.196	1.168	1.160	0.948
CH_4	0.002	0.007	0.007	0.000	0.000
Gas composition (mol%, N_2 and H_2O free)					
H_2	65.82	65.60	65.60	69.63	67.66
CO	5.46	5.93	5.93	2.60	3.56
CO_2	28.55	28.02	28.02	27.72	28.67
CH_4	0.14	0.45	0.45	0.00	0.00

regardless of the Cu content, ca. 0.004 mol H_2/(min m^2 Ni). These calculations corroborate the dilution effect of Cu in the catalysts.

3.2.2. Effect of the reduction time

The effect of the reduction time was studied with the 0% and 5% Cu catalysts. As already explained, the results from characterization by H_2 chemisorption indicated a noticeable increase in the Ni surface area of the 0% Cu catalyst when the reduction time was increased from 1 to 8 h. Therefore, it was decided to set a longer reduction time, 10 h, maintaining the rest of the reduction conditions.

The overall results of these experiments are presented in Table 6. Increasing the reduction time resulted in greater gas yields and carbon conversion to gas. Regarding yields to product gases, H_2, CO and CO_2 yields were substantially increased. The average gas composition showed little change.

The evolution of H_2 and CH_4 yields with reaction time are depicted in Figs. 5 and 6, respectively. The evolution of CO and CO_2 yields with time followed the same tendencies as H_2 and thus they are not depicted. The improvement in H_2 yield compared to the corresponding runs with 1 h of reduction time is significant, especially in the case of 0% Cu. A decrease is observed in the CH_4 yield when the reduction time increases.
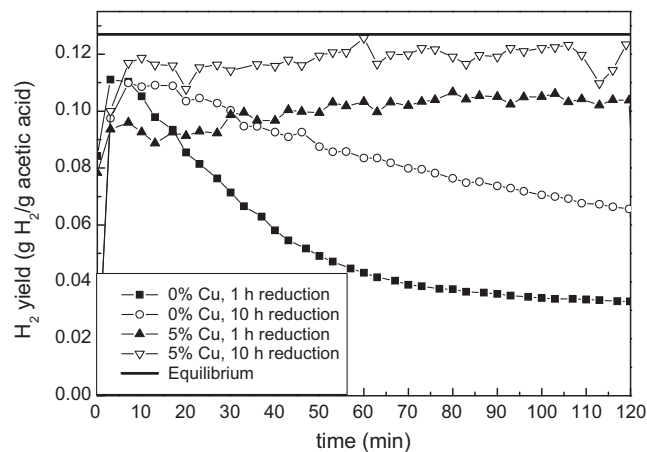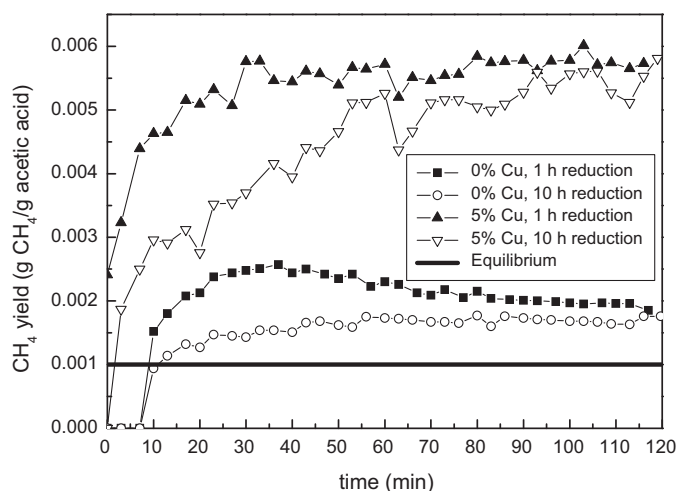

Fig. 5. H_2 yield evolution with time, effect of reduction time (lines between dots only represent visual aids). Temperature = 650 °C, W/m_{HAc} = 1.00 g catalyst min/g acetic acid (G_{C1}HSV = 41,660 h^{-1}), S/C = 5.6.

Fig. 6. CH$_4$ yield evolution with time, effect of reduction time (lines between dots only represent visual aids). Temperature = 650 °C, W/m_{HAc} = 1.00 g catalyst min/g acetic acid (G$_{C1}$ HSV = 41,660 h^{-1}), S/C = 5.6.

The 5% Cu catalyst seems to have a very stable performance throughout, with noticeable H$_2$ yields. Thus, it was considered of interest to perform a long time-on-stream (TOS) experiment with this catalyst. The catalytic steam reforming was done with the 5% Cu sample reduced during 10 h. The overall results of this long TOS experiment are also presented in Table 6. The carbon conversion to gas was nearly complete throughout, emphasizing the outstanding performance of this catalyst in the catalytic steam reforming of acetic acid at 650 °C through 12 h, run 8.

The performance of the catalyst in the long TOS experiment is very stable throughout, and the yields of the product gases are very close to their corresponding equilibrium values.

In order to explain these results, the characterization of some of the samples used was completed. XRD and TPO analyses were carried out, and some SEM images were taken. The samples selected were those employed in runs 6 and 7.

The TPO analyses revealed that different types of surface carbonaceous deposits were found in the steam reforming over Ni/Al catalysts. The results of these analyses indicate that the amount of carbon deposited on 0% Cu and 5% Cu catalysts are 19.4 and 36.8 g C/g sample (%), respectively.

The profiles of the TPO curves depicted in Fig. 7 show a peak at temperatures ranging from 620 to 650 °C for both samples. 0% Cu
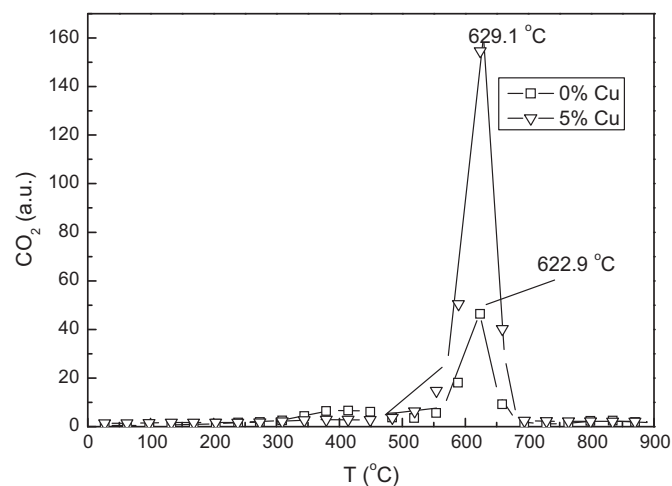

Fig. 7. TPO profiles of the samples corresponding to 0% Cu and 5% Cu catalysts used in runs 6 and 7, respectively.
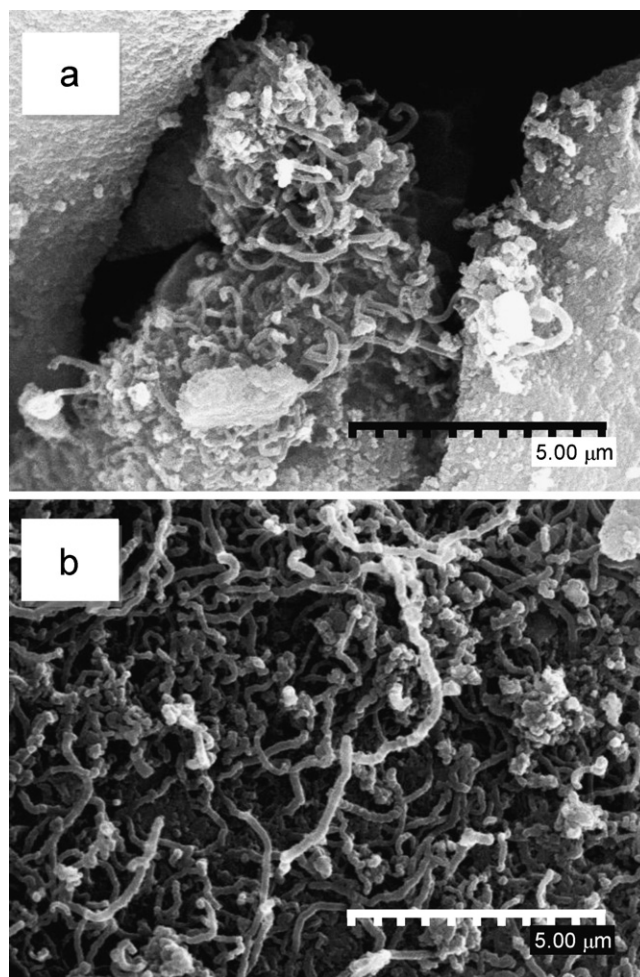

Fig. 8. SEM images of (a) the used 0% Cu sample corresponding to run 6 and (b) the used 5% Cu sample corresponding to run 7.

shows a larger and broader peak at temperatures between 400 and 440 °C. Interestingly, the 5% Cu sample does not seem to present a peak in that temperature range, showing a single peak in the whole profile.

The peak at temperatures around 620–650 °C can be attributed to filamentous carbon, whereas the peaks at relatively low temperatures, 350–440 °C, are ascribed to coke containing hydrogen (CH$_x$ species) and/or surface carbon [44,46]. Therefore, both samples seem to present mostly carbon deposited as filaments that are formed by surface atomic carbon on the front Ni surface, and segregation, diffusion and precipitation on the rear side of the Ni particles. The 0% Cu catalyst presents peaks corresponding to more reactive surface carbon, which could block the active surface sites resulting in a relatively fast deactivation.

Fig. 8 depicts the SEM images corresponding to the samples of the (a) 0% Cu and (b) 5% Cu catalysts used in runs 6 and 7, respectively. Both samples showed the presence of filamentous carbon. Longer and thicker whiskers are observed for the 5% Cu sample. These images are concordant with the results obtained in the TPO analyses, which indicated that the 5% Cu had more carbon deposited on its surface, and confirming the presence of filamentous coke deposited on both catalysts.

Fig. 9 shows the XRD patterns of the samples used. The main intensities of the patterns corresponding to standard Ni, NiO, MgO, and C (graphite) have also been included and appear as open and solid symbols. The XRD pattern of the 5% Cu sample clearly shows the presence of a broad peak at a diffraction angle 2θ equal to 26.6°,
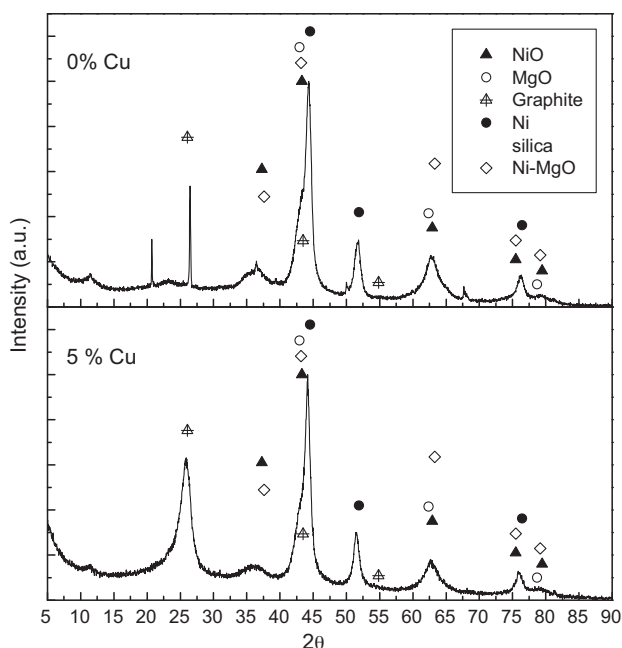
Fig. 9. XRD patterns of the 0% Cu and 5% Cu used samples corresponding to runs 6 and 7, respectively.

Fig. 10. H_2, and CO yield evolution with time. Effect of the S/C ratio at 650 °C, $W/m_{HAc} = 1.00$ g catalyst min/g acetic acid (lines between dots only represent visual aids).

which can be ascribed to carbon. Unfortunately, the XRD pattern of the 0% Cu sample presents an overlap with silica peaks that makes it impossible to confirm the presence of carbon deposited on this sample. The presence of silica, confirmed by the crystalline peaks at 2θ equal to 20.9°, may be due to an inadequate separation of the catalyst particles from the bed samples containing sand as inert filler.

Both the 0% and 5% Cu catalysts show broad peaks at characteristic diffraction angles of NiO, 2θ equal to 37.2°, 43.3° and 62.9°. In these samples metallic Ni can also be identified. The shoulder peaks at diffraction angles 2θ equal to 43.0°, 62.4° and 78.7° can be attributed to the presence of crystalline MgO. However, the presence of a Ni-MgO phase is also feasible. Little differences in the XRD patterns regarding Ni and oxides phases can be observed for 0% Cu and 5% Cu samples. Given the greater reducibility of 5% Cu catalyst, this result could be a consequence of the high reduction time employed.

From the results and the characterization of the used samples, it can be concluded that two types of carbon were deposited on the catalyst: a carbon deposited on the surface, which consists of carbon layers which can be easily oxidized, and a filamentous carbon which does not cause decay in the catalyst activity. The filamentous carbon could cause a loss in active phase after a regeneration step, since the formation of this type of carbon implies a raising of the Ni crystallite and its separation from the catalyst support [76]. The presence of Cu seems to diminish the formation of carbon layers, but not the formation of the filamentous carbon.

The role of copper in these catalysts can be deduced from the characterization analyses (TPO, SEM and XRD) of the used samples. The 5% Cu catalyst does not present a TPO peak at around 400–440 °C, which indicates no carbon layers are formed. Given that for the 5% Cu catalyst H_2, CO and CO_2 yields do not decrease with time, the carbon layers must be responsible for the catalyst deactivation observed in the 0% Cu catalyst. Other authors have proposed that copper inhibits the formation of graphite layers [50,58].

3.2.3. Effect of the steam-to-carbon (S/C) ratio

The effect of the S/C ratio was investigated with the 0% and 5% Cu catalysts reduced at 650 °C during 10 h. The results are presented
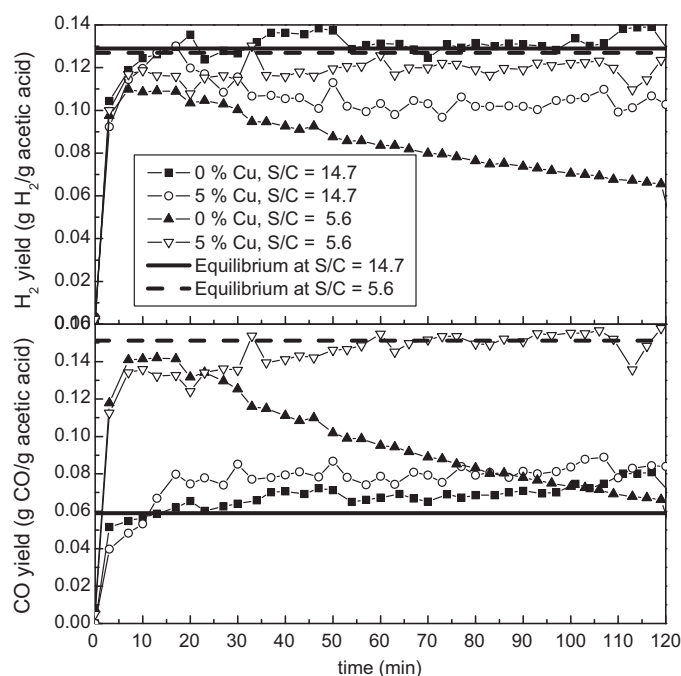
in Table 6. In the case of the 0% Cu catalyst, the results showed an enhanced carbon conversion to gases as well as greater yields to H_2, and CO_2, while the CO yield decreased when using the greater S/C ratio. In contrast, the 5% Cu catalyst yielded less carbon conversion to gas with a greater S/C ratio, while the individual yields to H_2, CO and CO_2 decreased, especially in the case of CO. Regarding gas composition, an increase in H_2 content and a decrease in CO and CO_2 is observed with a higher S/C ratio for 0% Cu, whereas for 5% Cu a slight increase in H_2 and CO_2 contents and a decrease in CO can be appreciated.

The evolution of H_2 and CO yields with time for these runs is presented in Fig. 10. Again, the CO_2 yields follow the same tendencies as H_2 and thus they have not been depicted. The high S/C (14.7) ratio improved the catalyst stability of the 0% Cu catalyst compared to that with a S/C of 5.6, most likely through reducing coke formation. Both H_2 and CO yields are close to equilibrium conditions, suggesting that the WGS reaction approaches equilibrium. The same tendency was also found for the 5% Cu catalyst. The conversion is only slightly lower at the high S/C ratio.

SEM images of the samples used in runs 9 and 10 are shown in Fig. 11(a) and (b), respectively. As occurred in the case of S/C = 5.6 (Fig. 8), the presence of filamentous carbon can be observed in both samples. Very short and thin whiskers are observed for the 0% Cu catalyst using a S/C = 14.7, whereas very long filaments are observed for the 5% Cu catalyst at the high S/C ratio. The results at both low and high S/C ratios indicate that the presence of Cu in the Ni catalysts enhanced filamentous carbon formation. The carbon formation affinity of acetic acid is so high that a S/C ratio as high as 14.7 could not prevent the formation of filaments.

3.3. Catalytic steam reforming of acetol and butanol

The overall results for the runs conducted with acetol and butanol as model compounds are presented in Table 7. These show a better performance with the 0% Cu catalyst, with almost complete carbon conversion to gases in the case of acetol. The yields to H_2, CO and CO_2 are close to the equilibrium values, though small amounts
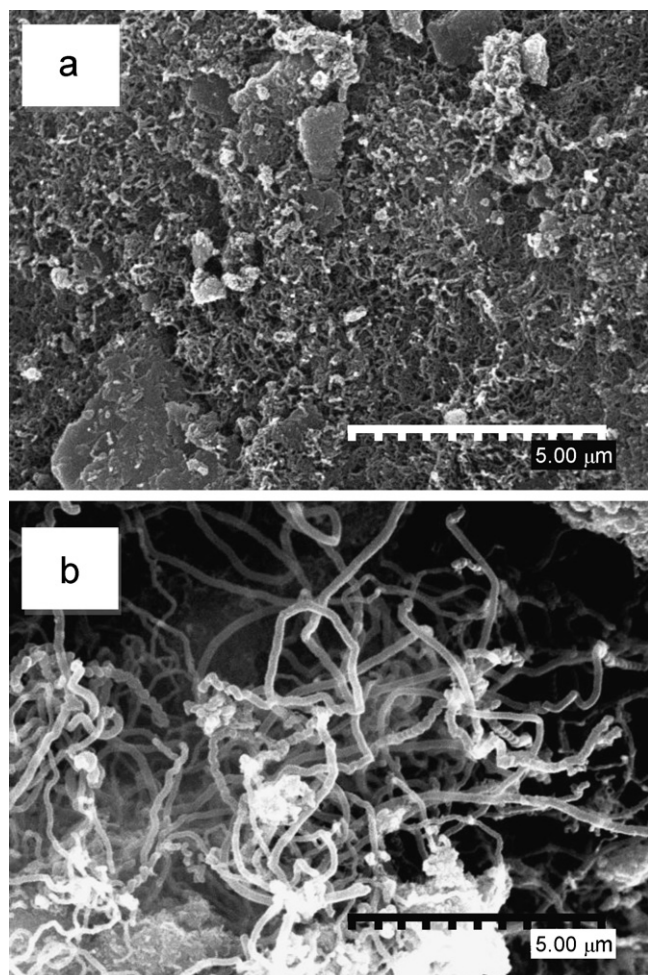
Fig. 11. SEM images of (a) the used 0% Cu sample with S/C = 14.7 (run 9), (b) the used 5% Cu sample with S/C = 14.7 (run 10).

Table 7
Overall results during 2 h of catalytic steam reforming of acetol and butanol at 650 °C. Effect of the Cu content. Acetol: catalyst weight: 18.1 mg, W/m_{Ac} = 0.53 g min/g acetol, G_{C1}HSV = 95,000 h^{-1}. Butanol: catalyst weight = 14.6 mg, W/m_{But} = 1.00 g catalyst min/g butanol, G_{C1}HSV = 67,000 h^{-1}.

|	Run			
	11	12	13	14
Organic	Acetol	Acetol	Butanol	Butanol
S/C	5.6	5.6	14.7	14.7
Catalyst	0% Cu	5% Cu	0% Cu	5% Cu
W/m_{org} (g$_{cat}$ min/g$_{org}$)	0.53	0.53	1.00	1.00
Copper content (%)	0	5	0	5
Yields (g/g liquid fed)				
Gas	0.350	0.288	0.118	0.072
Liquid	0.602	0.671	0.853	0.886
Recovery	0.952	0.959	0.970	0.958
Carbon conversion (%)	97.93	85.40	70.35	45.81
Gas yields (g/g organic)				
H_2	0.171	0.143	0.233	0.148
CO	0.214	0.248	0.154	0.186
CO_2	1.376	1.045	1.414	0.755
CH_4	0.012	0.024	0.000	0.006
C_2	0.001	0.007	0.003	0.007
Gas composition (mol%, N_2 and H_2O free)				
H_2	68.33	67.53	75.44	75.00
CO	5.93	8.26	3.55	6.87
CO_2	25.08	22.52	20.88	17.39
CH_4	0.59	1.44	0.00	0.39
C_2	0.05	0.24	0.11	0.32
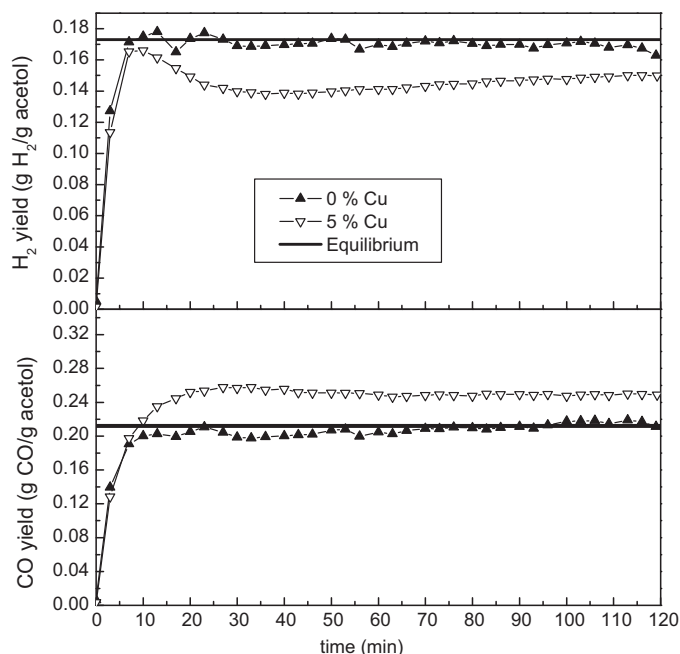
Fig. 12. H_2, and CO yield evolution with time, effect of copper content in catalytic steam reforming of acetol. T = 650 °C, W/m_{Ac} = 0.53 g catalyst min/g acetol (lines between dots only represent visual aids).

of CH_4 and C_2 were also detected. The 5% Cu catalyst shows less carbon conversion to gas than the 0% Cu catalyst for acetol and butanol. This could be due to Cu showing no activity for C—C bond cracking. However, other reactions could be favored and possibly other products (not analyzed) could be formed, as occurred in the steam reforming of acetic acid [66].

The CO, CH_4 and C_2 yields were greater than in the case of 0% Cu. The gas compositions followed the same tendencies. Thus, the presence of Cu seems not to be beneficial for the catalytic steam reforming of these model compounds, since at relatively high G_{C1}HSV values the 0% Cu catalyst yields greater carbon conversion as well as greater and more constant H_2 and CO_2 yields throughout.

The evolution of H_2 and CO yields with reaction time can be observed in Figs. 12 and 13 for acetol and butanol, respectively. The CO_2 yields follow the same tendencies as H_2, and thus they have not been depicted. Both for acetol and butanol, the 5% Cu catalyst depicted an initial decay in H_2 yield, though a smooth increase occurred after about 30 min of reaction time and the values are below equilibrium. On the other hand, the CO yield progressively increased up to a constant value after around 20 min of reaction time and the values are well above equilibrium.

For acetol, the 0% Cu catalyst shows stable H_2 and CO yields which are similar to equilibrium. However, for butanol the H_2 yield is smaller than the equilibrium value and a small decay can be observed.

The evolution of the CH_4 yield with time has also been depicted both for acetol and butanol (Fig. 14). It can be observed that the CH_4 yield is greater for the 5% Cu catalyst than the 0% Cu in both cases. Interestingly, the CH_4 yield is much lower for both catalysts in the steam reforming of butanol, being negligible when the 0% Cu catalyst was used.

The results of the non catalytic experiments with acetol and butanol at 650 °C were reported previously [35]. The methane content in the overall product gas compositions (% mol, N_2 and H_2O free) during 2 h were 6.7% for acetol and 2.7% for butanol. The overall C_2 contents in those experiments were 2.1% for acetol and 5.4% for butanol. These results again indicate that methane would be produced from the thermal decomposition of the model compound
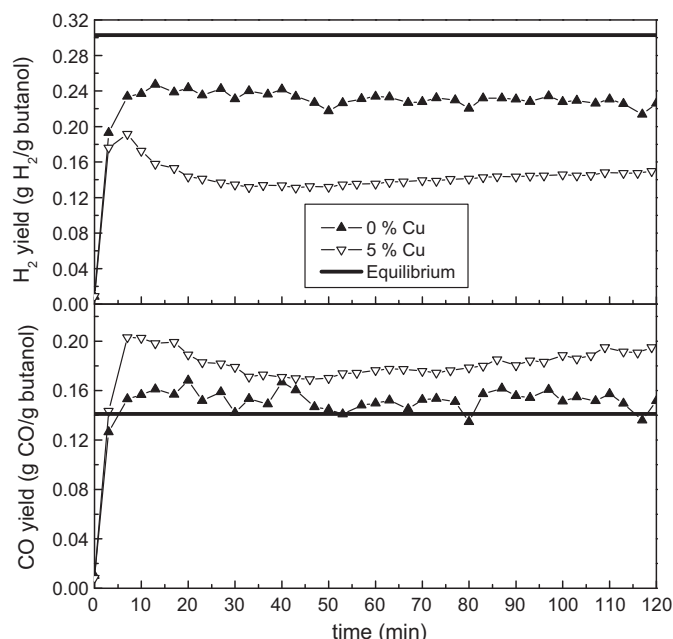
Fig. 13. H_2, and CO yield evolution with time, effect of copper content. $T = 650\,°C$, $W/m_{But} = 1.00$ g catalyst min/g butanol (lines between dots only represent visual aids).

and, in the presence of non-deactivated catalyst, it would be steam reformed.

These results indicate a higher activity of the 0%Cu catalyst in the steam reforming of methane (2) than that of the 5% Cu catalyst. This could be a consequence of the Cu-rich phase present in the 5% Cu catalyst.

The different results obtained in the catalytic steam reforming of acetic acid, acetol and butanol with Ni-Al catalysts modified with Cu could be a consequence of two opposite effects: on the one hand, Cu inhibits the formation of encapsulating coke that deactivates the catalysts, whereas on the other hand Cu also reduces the initial

Fig. 14. CH_4 yield evolution with time in acetol and butanol steam reforming, effect of copper content (lines between dots only represent visual aids).

reforming activity of the catalyst. Combining these two tendencies, the different behavior of the 0% and 5% Cu catalysts in the catalytic steam reforming of acetic acid, butanol and acetol could be explained. Acetic acid with a $S/C = 5.6$ seems to have a greater tendency to form coke than acetol or butanol. This is deduced from the carbon conversion decay with reaction time using the same catalyst and space velocity [35]. The greater reactivity in the case of acetol and the high S/C ratio in the butanol solution must be the cause [35]. The beneficial effect of inhibiting encapsulating coke by Cu is therefore irrelevant with acetol and butanol and acetic acid with $S/C = 14.7$. The initial reforming activity of the catalyst is reduced due to the Ni dilution effect by the Cu, as was determined in the chemisorption measurements.

4. Conclusions

The catalytic steam reforming of model compounds (acetic acid, acetol and butanol) from biomass pyrolysis oil has been studied at $650\,°C$ and atmospheric pressure using Ni/Al coprecipitated catalysts modified with magnesium and copper. The most relevant conclusions from the present work are the following:

1. Steam reforming of acetic acid ($S/C = 5.6$) using the catalysts reduced at $650\,°C$ during 1 h shows a stable performance for 5% Cu and 10% Cu catalysts, while 0% Cu, 1% Cu and 3% Cu catalysts deactivate rapidly.
2. In the steam reforming of acetic acid, the addition of Cu as a promoter enhances the catalyst stability. This enhancement could be attributed to copper inhibiting the deposition of encapsulating coke on the catalyst surface. However, the presence of Cu increases the formation of filamentous carbon.
3. The addition of Cu diminishes the Ni surface area. The initial steam reforming activity is decreased, which is probably due to the Ni dilution effect caused by copper.
4. A high reforming activity and stable performance were obtained in the steam reforming of acetic acid ($S/C = 5.6$) during 12 h of reaction at a short space time (1.00 g catalyst min/g acetic acid) using the 5% Cu catalyst reduced during 10 h at $650\,°C$.
5. The 0% Cu catalyst shows a better performance than the 5% Cu catalyst, with higher reforming activity in the steam reforming of acetic acid with $S/C = 14.7$, the steam reforming of acetol ($S/C = 5.6$) and in the steam reforming of butanol ($S/C = 14.7$).

Acknowledgements

References

[1] J. Diebold, J. Scahill, ACS Symp. Ser. 376 (1988) 31–40.
[2] D. Radlein, J. Piskorz, D.S. Scott, J. Anal. Appl. Pyrolysis 19 (1991) 41–63.
[3] A.V. Bridgwater, G.V.C. Peacocke, Ren. Sust. Energ. Rev. 4 (2000) 1–73.
[4] A. Bridgwater, Therm. Sci. 8 (2004) 21–49.
[5] S. Czernik, A. Bridgwater, Energy Fuels 18 (2004) 590–598.
[6] C. Briens, J. Piskorz, F. Berruti, Int. J. Chem. React. Eng. 6 (2008) R2.
[7] D. Wang, S. Czernik, D. Montane, M. Mann, E. Chornet, Ind. Eng. Chem. Res. 36 (1997) 1507–1518.
[8] A. Oasmaa, D. Meier, J. Anal. Appl. Pyrol. 73 (2005) 323–334.
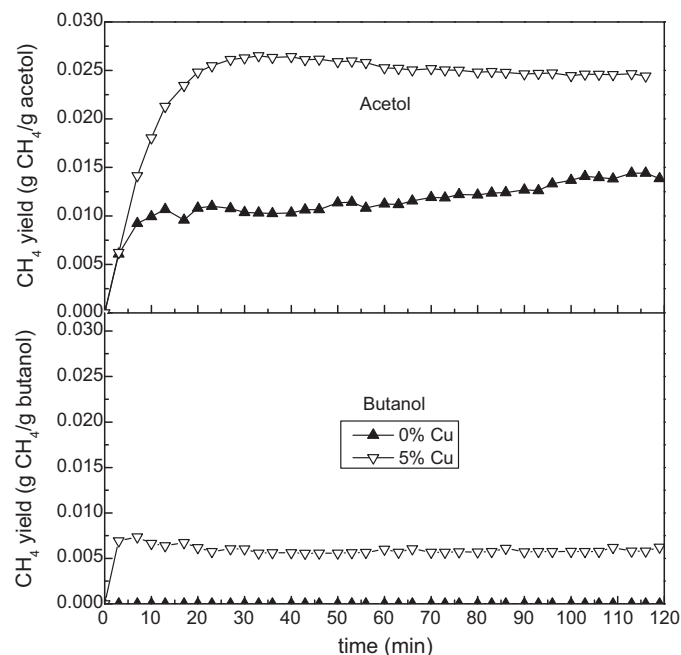[9] J. Piskorz, D. Scott, D. Radlein, ACS Symp. Ser. 376 (1988) 167–178.

[10] J. Adjaye, N.N. Bakhshi, Biomass Bioenerg. 8 (1995) 131–149.
[11] D. Wang, D. Montane, E. Chornet, Appl. Catal. A: Gen. 143 (1996) 245–270.
[12] J.R. Galdámez, L. García, R. Bilbao, Energy Fuels 19 (2005) 1133–1142.
[13] C. Rioche, S. Kulkarni, F.C. Meunier, J.P. Breen, R. Burch, Appl. Catal. B: Environ. 61 (2005) 130–139.
[14] S. Duan, S. Senkan, Ind. Eng. Chem. Res. 44 (2005) 6381–6386.
[15] X. Hu, G. Lu, Chem. Lett. 35 (2006) 452–453.
[16] A.C. Basagiannis, X.E. Verykios, Appl. Catal. A: Gen. 308 (2006) 182–193.
[17] K. Takanabe, K. -ichi Aika, K. Inazu, T. Baba, J. Catal. 263 (2006) 263–269.
[18] K. Takanabe, K. -ichi Aika, K. Seshan, L. Lefferts, Chem. Eng. J. 120 (2006) 133–137.
[19] P.N. Kechagiopoulos, S.S. Voutetakis, A.A. Lemonidou, I.A. Vasalos, Energy Fuels 20 (2006) 2155–2163.
[20] F. Bimbela, M. Oliva, J. Ruiz, L. García, J. Arauzo, J. Anal. Appl. Pyrolysis 79 (2007) 112–120.
[21] E.C. Vagia, A.A. Lemonidou, Int. J. Hydrogen Energy 33 (2008) 2489–2500.
[22] X. Hu, G. Lu, J. Mol. Catal. A: Chem. 261 (2007) 43–48.
[23] A.C. Basagiannis, X.E. Verykios, Int. J. Hydrogen Energy 32 (2007) 3343–3355.
[24] A.C. Basagiannis, X.E. Verykios, Catal. Today 127 (2007) 256–264.
[25] T. Davidian, N. Guilhaume, C. Daniel, C. Mirodatos, Appl. Catal. A: Gen. 335 (2008) 64–73.
[26] T. Davidian, N. Guilhaume, H. Provendier, C. Mirodatos, Appl. Catal. A: Gen. 337 (2008) 111–120.
[27] P.N. Kechagiopoulos, S.S. Voutetakis, A.A. Lemonidou, I.A. Vasalos, Ind. Eng. Chem. Res. 48 (2009) 1400–1408.
[28] J.A. Medrano, M. Oliva, J. Ruiz, L. García, J. Arauzo, J. Anal. Appl. Pyrolysis 85 (2009) 214–225.
[29] B. Matas Güell, I.M.T. Silva, K. Seshan, L. Lefferts, Appl. Catal. B: Environ. 88 (2009) 59–65.
[30] B. Matas Güell, I. Babich, K.P. Nichols, J.G.E. Gardeniers, L. Lefferts, K. Seshan, Appl. Catal. B: Environ. 90 (2009) 38–44.
[31] X. Hu, G. Lu, Appl. Catal. B: Environ. 88 (2009) 376–385.
[32] P.N. Kechagiopoulos, S.S. Voutetakis, A.A. Lemonidou, I.A. Vasalos, Catal. Today 127 (2007) 246–255.
[33] E.C. Vagia, A.A. Lemonidou, Appl. Catal. A: Gen. 351 (2008) 111–121.
[34] M.C. Ramos, A.I. Navascués, L. García, R. Bilbao, Ind. Eng. Chem. Res. 46 (2007) 2399–2406.
[35] F. Bimbela, M. Oliva, J. Ruiz, L. García, J. Arauzo, J. Anal. Appl. Pyrolysis 85 (2009) 204–213.
[36] D. Wang, S. Czernik, E. Chornet, Energy Fuels 12 (1998) 19–24.
[37] M. Marquevich, R. Coll, D. Montane, Ind. Eng. Chem. Res. 39 (2000) 2140–2147.
[38] M. Marquevich, S. Czernik, E. Chornet, D. Montané, Energy Fuels 13 (1999) 1160–1166.
[39] M. Marquevich, F. Medina, D. Montané, Catal. Commun. 2 (2001) 119–124.
[40] L. García, R. French, S. Czernik, E. Chornet, Appl. Catal. A: Gen. 201 (2000) 225–239.
[41] T. Davidian, N. Guilhaume, E. Iojoiu, H. Provendier, C. Mirodatos, Appl. Catal. B: Environ. 73 (2007) 116–127.
[42] M. Marquevich, X. Farriol, F. Medina, D. Montane, Catal. Lett. 85 (2003) 41–48.
[43] K. Takanabe, K. -ichi Aika, K. Seshan, L. Lefferts, J. Catal. 227 (2004) 101–108.
[44] A. Djaidja, S. Libs, A. Kiennemann, A. Barama, Catal. Today 113 (2006) 194–200.
[45] A. Monzón, N. Latorre, T. Ubieto, C. Royo, E. Romeo, J.I. Villacampa, L. Dussault, J.C. Dupin, C. Guimon, M. Montioux, Catal. Today 116 (2006) 264–270.
[46] J. da, S. Lisboa, D.C.R.M. Santos, F.B. Passos, F.B. Noronha, Catal. Today 101 (2005) 15–21.
[47] K. Christensen, Steam Reforming of Methane on Different Nickel Catalysts, Norges Teknisk Naturvitenskapelige Universitet, 2005.
[48] L. García, A. Benedicto, E. Romeo, M.L. Salvador, J. Arauzo, R. Bilbao, Energy Fuels 16 (2002) 1222–1230.
[49] L. He, H. Berntsen, E. Ochoa-Fernández, J.C. Walmsley, E.A. Blekkan, D. Chen, Top. Catal. 52 (2009) 206–217.
[50] N.M. Rodriguez, M.S. Kim, R.T.K. Baker, J. Catal. 140 (1993) 16–29.
[51] L.B. Avdeeva, O.V. Goncharova, D.I. Kochubey, V.I. Zaikovskii, L.M. Plyasova, B.N. Novgorodov, S.K. Shaikhutdinov, Appl. Catal. A: Gen. 141 (1996) 117–129.
[52] V.B. Fenelonov, A.Y. Durevyankin, L.G. Okkel, L.B. Avdeeva, V.I. Zaikovskii, E.M. Moroz, A.N. Salanov, N.A. Rudina, V.A. Likholobov, S.K. Shaikhutdinov, Carbon 35 (1997).
[53] Y. Li, J. Chen, L. Chang, Y. Qin, J. Catal. 178 (1998) 76–83.
[54] T.V. Reshetenko, L.B. Avdeeva, Z.R. Ismagilov, A.L. Chuvilin, V.A. Ushakov, Appl. Catal. A: Gen. 247 (2003) 51–63.
[55] J. Chen, Y. Li, Z. Li, X. Zhang, Appl. Catal. A: Gen. 269 (2004) 179–186.
[56] A.R. Naghash, T.H. Etsell, S. Xu, Chem. Mater. 18 (2006) 2480–2488.
[57] Y. Echegoyen, I. Suelves, M.J. Lázaro, R. Moliner, J.M. Palacios, J. Power Sources 169 (2007) 150–157.
[58] Y. Echegoyen, I. Suelves, M.J. Lázaro, M.L. Sanjuán, R. Moliner, Appl. Catal. A: Gen. 333 (2007) 229–237.
[59] R. Moliner, Y. Echegoyen, I. Suelves, M.J. Lázaro, J. Palacios, Int. J. Hydrogen Energy 33 (2008) 1719–1728.
[60] J. Ashok, M. Subrahmanyam, A. Venugopal, Int. J. Hydrogen Energy 33 (2008) 2704–2713.
[61] L. Dussault, J. Dupin, C. Guimon, M. Monthioux, N. Latorre, T. Ubieto, E. Romeo, C. Royo, A. Monzón, J. Catal. 251 (2007) 223–232.
[62] F.J. Mariño, E.G. Cerrella, S. Duhalde, M. Jobbagy, M.A. Laborde, Int. J. Hydrogen Energy 23 (1998) 1095–1101.
[63] F.J. Mariño, M. Boveri, G. Baronetti, M. Laborde, Int. J. Hydrogen Energy 26 (2001) 665–668.
[64] F.J. Mariño, G. Baronetti, M. Jobbagy, M. Laborde, Appl. Catal. A: Gen. 238 (2003) 41–54.
[65] F.J. Mariño, M. Boveri, G. Baronetti, M. Laborde, Int. J. Hydrogen Energy 29 (2004) 67–71.
[66] X. Hu, G. Lu, Appl. Catal. B: Environ. 99 (2010) 289–297.
[67] A. Bhattacharyya, W.D. Chang, M.S. Kleefisch, C.A. Udovic, US Patent 5767040 (1998).
[68] Z. Yu, D. Chen, M. Ronning, T. Vraalstad, E. Ochoa-Fernández, A. Holmen, Appl. Catal. A: Gen. 338 (2008) 136–146.
[69] R.H. Perry, D.W. Green (Eds.), Perry's Chemical Engineers' Handbook, 7th ed., McGraw-Hill, 1999.
[70] J.A. Peña, J. Herguido, C. Guimon, A. Monzón, J. Santamaría, J. Catal. 159 (1996) 313–322.
[71] L. García, M.L. Salvador, R. Bilbao, J. Arauzo, Energy Fuels 12 (1998) 139–143.
[72] Y. Cesteros, P. Salagre, F. Medina, J.E. Sueiras, Chem. Mater. 12 (2000) 331–335.
[73] P. Salagre, J.L.G. Fierro, F. Medina, J.E. Sueiras, J. Mol. Catal. A: Chem. 106 (1996) 125–134.
[74] J.A. Anderson, M. Fernández-García, A. Martínez-Arias, in: J. Anderson, M. Fernández-García (Eds.), Supported Metals in Catalysis, Imperial College Press, London, 2005, pp. 145–146.
[75] S. Czernik, R. Evans, R. French, Catal. Today 129 (2007) 265–268.
[76] J. Villacampa, C. Royo, E. Romeo, J.A. Montoya, P. Del Ángel, A. Monzón, Appl. Catal. A: Gen. 252 (2003) 363–383.